

1 [RESEARCH ARTICLE]

2 **pH Gradient Mitigation in the Leaf Cell Secretory Pathway Alters the**
3 **Defense Response of *Nicotiana benthamiana* to Agroinfiltration**

4 Philippe V. Jutras ^a, Frank Sainsbury ^b, Marie-Claire Goulet ^a, Pierre-Olivier Lavoie ^c, Rachel
5 Tardif ^c, Louis-Philippe Hamel ^c, Marc-André D'Aoust ^c, and Dominique Michaud^{a*}

6 ^a *Centre de recherche et d'innovation sur les végétaux, Université Laval, Québec, Canada*

7 ^b *The University of Queensland, Australian Institute for Bioengineering and Nanotechnology, St*
8 *Lucia, Australia*

9 ^c *Medicago Inc., Québec, Canada*

10

11 * *Corresponding author (dominique.michaud@fsaa.ulaval.ca)*

Philippe V. Jutras et al.

12 **ABSTRACT**

13 Partial neutralization of the Golgi lumen pH by ectopic expression of influenza virus M2 proton
14 channel stabilizes acid-labile and protease-susceptible recombinant proteins in the plant cell
15 secretory pathway. Here, we assessed the impact of M2 channel expression on the proteome of
16 *Nicotiana benthamiana* leaf tissue infiltrated with the bacterial gene vector *Agrobacterium*
17 *tumefaciens*, keeping in mind the key role of pH homeostasis on secreted protein processing and
18 the involvement of protein secretion processes in plant cells upon microbial challenge. The
19 proteomes of leaves agroinfiltrated with an empty vector or with an M2 channel-encoding vector
20 were compared with the proteome of non-infiltrated leaves using a iTRAQ quantitative proteomics
21 procedure. Leaves infiltrated with the empty vector had a low soluble protein content compared
22 to non-infiltrated leaves, associated with a strong decrease of photosynthesis-associated proteins
23 (including Rubisco) and a parallel increase of stress-related secreted proteins (including
24 pathogenesis-related proteins, protease inhibitors and molecular chaperones). M2 expression
25 partly compromised these alterations of the proteome to restore original soluble protein and
26 Rubisco contents, associated with higher levels of translation-associated (ribosomal) proteins and
27 reduced levels of stress-related proteins in the apoplast. Proteome changes in M2-expressing
28 leaves were determined both transcriptionally and post-transcriptionally, to alter the steady-state
29 levels of proteins not only along the secretory pathway but also in other cellular compartments
30 including the chloroplast, the cytoplasm, the nucleus and the mitochondrion. These data illustrate
31 the cell-wide influence of Golgi lumen pH homeostasis on the leaf proteome of *N. benthamiana*
32 plants responding to microbial challenge. They underline in practice the relevance of carefully
33 considering the eventual off-target effects of accessory proteins used to modulate specific cellular
34 or metabolic functions in plant protein biofactories.

35 **Keywords** – iTRAQ, shotgun quantitative proteomics, *Nicotiana benthamiana*, influenza virus
36 M2 proton channel, defense response, photosynthesis, leaf agroinfiltration

Philippe V. Jutras et al.

37 INTRODUCTION

38 Major advances in plant cell biology and genetic engineering have bolstered the use of plants as
39 expression hosts for clinically and industrially valuable recombinant proteins (Stöger et al., 2014;
40 Sack et al., 2015; Lomonosoff and D'Aoust, 2016; Tschofen et al., 2016). An array of DNA
41 vectors, regulatory sequences and delivery systems have been developed for high-level
42 transgene expression in plant systems (Streatfield, 2007; Makhzoum et al., 2014). Basic
43 knowledge on protein biosynthetic pathways in plants has been translated in parallel to plant
44 expression hosts, helpful to sustain proper maturation of expressed proteins or to implement novel
45 cellular functions for effective protein processing *in planta* (Faye et al., 2005; Gomord et al., 2010;
46 Mandal et al., 2016). Current efforts to further strengthen the position of plants as valuable protein
47 expression hosts also include the development of metabolic, cellular or phenology engineering
48 approaches to address specific issues related to recombinant protein maturation, stability or
49 recovery. Examples are the ectopic implementation of a dwarf plant phenotype to optimize culture
50 area use in the greenhouse (Nagatoshi et al., 2015), activation of the octadecanoid pathway to
51 reduce ribulose 1,5-*bis*-phosphate carboxylase oxygenase (Rubisco) loads in leaves prior to
52 protein purification (Robert et al., 2015), or the expression of accessory convertases to generate
53 biologically active forms of therapeutic proteins otherwise requiring chemical refolding after
54 extraction (Wilbers et al., 2016). Other examples are the expression of protease inhibitors to
55 prevent unintended protein degradation by resident proteases (Goulet et al., 2012; Pillay et al.,
56 2014; Jutras et al., 2016), or the expression of an accessory proton channel to stabilize acid-labile
57 and proteolysis-susceptible proteins in the Golgi lumen (Jutras et al., 2015; 2018).

58 A key challenge now to harness the full potential of these emerging engineering approaches
59 and to take advantage of their eventual synergistic effects *in planta* is to decipher their possible
60 'off-target' effects *in planta*. By definition, rational schemes for plant metabolic engineering target
61 specific physiological or enzymatic processes but unintended effects in the modified host cannot
62 be ruled out, especially in those cases where the ectopic effectors alter basic cellular functions or
63 physicochemical parameters. For instance, the inhibition of host endogenous proteases with
64 accessory protease inhibitors is useful to prevent the degradation of protease-susceptible
65 recombinant proteins *in planta* (Robert et al., 2016) but interfering effects on protein biosynthetic
66 and turnover rates in the modified host could in some cases have an impact, positive or negative,
67 on overall protein yields recovered from source tissues (Badri et al., 2009; Goulet et al., 2010a).
68 Similarly, partial neutralization of the Golgi lumen pH by ectopic expression of influenza virus M2
69 proton channel (Holsinger et al., 1994) is useful to stabilize acid-labile proteins *in situ* (Jutras et

Philippe V. Jutras et al.

70 al., 2015) but eventual effects of this transporter on host physiological functions remain likely
71 given the influence of pH homeostasis on protein posttranslational maturation, processing and
72 trafficking along the cell secretory pathway (Schumacher, 2014; Jutras et al., 2018).

73 Our goal in this study was to assess the impact of M2 channel expression on the leaf proteome
74 of *Nicotiana benthamiana* infiltrated with the bacterial gene vector *Agrobacterium tumefaciens*.
75 M2 forms tetrameric transmembrane channels for proton extrusion in the cytosol of infected
76 mammalian cells, to generate an increased pH in the Golgi lumen favourable to the folding and
77 stability of the influenza virus glycoproteins (Schnell and Chou, 2008; Cady et al., 2009). Transient
78 expression of M2 in *N. benthamiana* leaves was shown to trigger a similar pH increase in the *cis*-
79 and *trans*-Golgi compartments, useful to stabilize acid-labile recombinant proteins and peptide
80 linkers migrating towards to the apoplast (Jutras et al., 2015). A side effect of the viral transporter
81 was also reported recently, by which the activity of pH-dependent resident proteases and their
82 impact on the integrity of protease-susceptible proteins in the secretory pathway is altered upon
83 pH increase (Jutras et al., 2018). An unsolved question at this point is to what extent M2
84 expression exerts pleiotropic effects on host plant cellular functions via its primary effect on pH
85 homeostasis in the secretory pathway. As in other eukaryotic cells (Orlowski and Grinstein, 2011),
86 a pH gradient is naturally established in plant cells between the ER and the Golgi (Martinière et
87 al., 2013; Shen et al., 2013) by the combined action of V-type H⁺-ATPases for lumen acidification
88 and Na⁺/H⁺ antiporters for proton efflux and pH fine-tuning (Bassil and Blumwald, 2014). Early
89 transfection studies with animal cell models showed significant effects of M2 ectopic expression
90 on endogenous protein trafficking and Golgi cisternae morphology, presumably due to a disturbed
91 balance of 'in and out' proton movements through the Golgi membranes (Sakaguchi et al., 1996;
92 Henkel et al., 1998). Similarly, altered pH in the Golgi of Arabidopsis Na⁺/H⁺ antiporter knockouts,
93 or in the Golgi of plant cells treated with chemical inhibitors of V-type H⁺-ATPases or Na⁺/H⁺
94 antiporters, was associated with altered rates of protein posttranslational processing and
95 trafficking towards the late secretory pathway compartments (Dettmer et al., 2006; Martinière et
96 al., 2013; Ashnest et al., 2015; Reguera et al., 2015; Wu et al., 2016). We here followed
97 an 'isobaric tags for relative and absolute quantification' (iTRAQ) liquid chromatography (LC)-
98 mass spectrometry (MS/MS) approach (Brewis and Brennan, 2010) to probe the influence of
99 Golgi lumen pH homeostasis on the whole proteome of agroinfiltrated *N. benthamiana* leaves
100 upon M2 expression, keeping in mind the significance of protein secretion and trafficking in plant
101 cells responding to microbial challenge (Inada and Ueda, 2014; Ben Khaled et al., 2015).

102

Philippe V. Jutras et al.

103 RESULTS AND DISCUSSION

104 Agroinfiltration Alters the Leaf Proteome of *N. benthamiana*

105 Total soluble proteins and total numbers of up- and downregulated proteins in whole-cell samples
106 were first determined to get a general overview of proteome alterations in leaves infiltrated either
107 with agrobacteria harboring an M2 channel-encoding vector, or with agrobacteria harboring an
108 'empty' version of the same vector (EV), to measure the effects of bacterial infiltration and M2
109 expression on leaf protein content at the cell-wide scale (**Fig. 1**). A significant adjustment of the
110 protein complement was suggested by a low total soluble protein content of 5.7 mg.g⁻¹ fresh
111 weight in EV-infiltrated leaves compared to 9.4 mg.g⁻¹ in non-infiltrated leaves 6 d post-infiltration
112 (post-ANOVA LSD; $P < 0.05$) (**Fig. 1A**). Protein content reduction in agroinfiltrated leaves was
113 associated with a downregulation of ribulose-1,5-*bis*-phosphate carboxylase/oxygenase (Rubisco)
114 large and small subunits and a concomitant upregulation of protein bands in the 20–35-kDa range
115 (**Fig. 1B**). By contrast, protein content in M2 vector-infiltrated leaves was estimated at 8.4 mg.g⁻¹
116 fresh weight, statistically similar to non-infiltrated leaves (LSD; $P > 0.05$) (**Fig. 1A**). Rubisco subunit
117 band intensities were also comparable in M2 vector-infiltrated and non-infiltrated leaves, two to
118 three times more intense than the corresponding bands in EV-infiltrated leaves (**Fig. 1B**). A time-
119 course analysis over 12 d post-infiltration indicated a rapid and durable upregulating effect of M2
120 expression on soluble protein content compared to EV-infiltrated leaves, already measurable after
121 2 d and still important after 12 d (**Supplemental Fig. S1**). No positive effect on protein content
122 was observed in leaves infiltrated to express ^{A30P}M2, an inactive single mutant of M2 (Holsinger
123 et al., 1994) (**Supplemental Fig. S1**), indicating a link between the protein content-restoring effect
124 of the transporter and its proton-conducting activity in agroinfiltrated leaves.

125 We conducted a iTRAQ analysis of non-infiltrated and infiltrated leaf protein extracts to
126 estimate the overall impacts of agroinfiltration and M2 expression on the leaf soluble protein
127 complement (**Fig. 1C,D**) and to characterize the specific effects of these treatments at the cell-
128 wide scale (**Figs. 2–5**). A total of 5,928 unique peptides were detected by MS/MS, allowing for
129 the identification of 2,388 proteins at a confidence level of 95% ($P < 0,05$). A little more than 50%
130 (i.e. 1,255) of these proteins were identified based on at least two unique peptides and used for
131 further comparative assessments (**Supplemental Table S1**). On a leaf fresh weight (FW) basis,
132 425 proteins were downregulated, and 50 proteins upregulated, by at least twofold in EV-infiltrated
133 leaves compared to 214 proteins downregulated and 54 upregulated in M2 vector-infiltrated
134 leaves (**Fig. 1C**). On a total soluble protein (TSP) basis, 202 proteins were downregulated, and
135 139 upregulated, in EV-infiltrated leaves compared to non-infiltrated leaves, roughly similar to

Philippe V. Jutras et al.

136 protein numbers flagged as down- (162) or upregulated (79) upon M2 expression (**Fig. 1C**). A
137 pairwise comparison of MS/MS data produced for EV- and M2 vector-infiltrated leaves was
138 performed to estimate the overall impact of M2 proton channel activity on agroinfiltration-induced
139 proteome changes (**Fig. 1D**). On a TSP basis, only 10 proteins were upregulated, and 19
140 downregulated, by at least twofold in M2 vector-infiltrated leaves compared to EV-infiltrated
141 leaves, out of 1,255 proteins monitored. These data suggested overall a qualitative impact of M2
142 expression on the host proteome limited, on protein-specific basis, to a relatively small number of
143 up- or downregulated proteins. They confirmed, by contrast, the strong impact of agroinfiltration
144 on the leaf proteome, attenuated to some extent by Golgi pH alteration in M2-expressing cells.

145 **Agroinfiltration Triggers a Classical Biotrophic Pathogen-Inducible Defense Response in** 146 **Leaves**

147 We performed BLAST alignments and a Gene Ontology (GO) enrichment analysis of our MS/MS
148 dataset to classify the most significant proteome alterations in agroinfiltrated leaves based on the
149 biological roles, biochemical functions and/or subcellular locations assigned *in silico* to the
150 regulated proteins (**Fig. 2, Supplemental Fig. S2**). Agroinfiltration was shown previously to
151 trigger the secretion of stress-related proteins in *N. benthamiana* leaves including salicylic acid-
152 inducible pathogenesis-related (PR) protein PR-1a and several PR-2 (β -glucanase), PR-3
153 (chitinase) and PR-5 (osmotin) protein isoforms (Pruss et al., 2008; Goulet et al., 2010b; Robert
154 et al., 2015). We here assigned biological roles and cellular locations to the 60 most upregulated,
155 and 60 most downregulated, proteins in EV-infiltrated plants representing, together, 10% of the
156 proteins confidently identified by MS/MS and 25% of the proteins up- or downregulated by at least
157 twofold in agroinfiltrated leaf tissue. In line with previous studies, a range of defense and oxidative
158 stress-related proteins were induced in EV-infiltrated leaves, including oxidoreductases (e.g.
159 peroxidases), molecular chaperones (e.g. heat shock proteins), PR proteins (e.g. β -glucanases,
160 chitinases, osmotins) and protease inhibitors (e.g. Kunitz proteins) (**Supplemental Table S2**).
161 Stress-related proteins accounted for approximately two thirds of the upregulated proteins (**Fig.**
162 **2A**, upper panel), distributed in several cellular compartments including the chloroplast, the
163 mitochondrion, the nucleus, the cytosol and different parts of the cell secretory pathway (**Fig. 2A**,
164 lower panel). Similar to conclusions drawn earlier for the leaf apoplast proteome (Goulet et al.,
165 2010b), all upregulated proteins in soluble protein samples, including chloroplastic proteins, were
166 nuclear genome-encoded (**Fig. 2A**, lower panel).

167 Unlike stress-related proteins, several proteins involved in mRNA translation, photosynthesis
168 and ATP biosynthesis were strongly downregulated in EV-infiltrated leaves (**Fig. 2B**, upper panel).

Philippe V. Jutras et al.

169 Chloroplastic proteins including Rubisco (also see **Fig. 1B**), structural subunits of photosystems
170 I and II, chlorophyll-binding proteins, ATP synthase subunits and translation-associated ribosomal
171 proteins (**Supplemental Table S3**) accounted for more than 75% of the downregulated proteins
172 (**Fig. 2B**, lower panel). A small proportion (13%) of these proteins were chloroplast genome-
173 encoded but the vast majority were encoded by the nuclear genome as observed for the
174 upregulated proteins (**Fig. 2B**, lower panel). These observations supported overall those current
175 experimental models suggesting the onset of growth–defense trade-offs in microbe-infected
176 plants, whereby energy production- and photosynthesis-associated genes are downregulated
177 upon microbial challenge (or ectopic application of salicylic acid) to limit the availability of carbon
178 resources to the invading organism or to promote defense responses over primary metabolism-
179 related processes (Sugano et al., 2010; Takatsuji, 2017). Our data showing an impact of
180 agroinfiltration at the whole cell scale also reminded the strong influence of pathogen infection on
181 nuclear gene expression and the likely implication of leaf chloroplasts as stress signal receivers
182 and pro-defense secondary signal transmitters to the nucleus upon microbial attack (Serrano et
183 al., 2016). Primary signals transmitted into plant cells to induce immune responses following
184 membrane receptor-mediated recognition of pathogen-associated molecular patterns (Boller and
185 Felix, 2009) are readily relayed to the chloroplasts, where they trigger the production of retrograde
186 secondary signals that move towards the nucleus to activate defense-related genes and repress
187 chloroplast protein-encoding genes (Nomura et al., 2012). Retrograde signals identified in recent
188 years were shown to induce nuclear genes involved in the biosynthesis of salicylic acid (Nomura
189 et al., 2012; Xiao et al., 2012; Ishiga et al., 2017), a key elicitor of immune responses to
190 agroinfiltration in *N. benthamiana* leaves (Anand et al., 2008; Pruss et al., 2008).

191 **M2 Channel Expression Attenuates the Host Plant Response to Agroinfiltration**

192 A complementary GO enrichment analysis was performed to characterize eventual interfering
193 effects of M2 expression on host leaf proteome adjustments upon agroinfiltration (**Fig. 3**,
194 **Supplemental Fig. S3**). Our observations above about the overall effects of EV and M2 vector
195 infiltrations (**Fig. 1**) suggested a limited impact of M2 on the proteome of agroinfiltrated plants as
196 expressed in numbers of proteins up- or downregulated by at least twofold in leaf tissue. By
197 contrast, they indicated a strong positive effect of the viral transporter on soluble leaf protein and
198 Rubisco contents that suggested a possibly attenuated defense response upon infection
199 associated with an alteration of pH gradient homeostasis along the cell secretory pathway. We
200 here addressed these questions by comparing the proteomes of EV- and M2 vector-infiltrated leaf
201 protein samples, considering the 60 most upregulated, and 60 most downregulated, proteins in

Philippe V. Jutras et al.

202 M2-expressing leaves relative to EV-infiltrated leaves taken as a control. Supporting the
203 hypothesis of a defense-attenuating effect for M2, chloroplast and nuclear genome-encoded
204 proteins downregulated in EV-infiltrated leaves were found at higher levels in M2-expressing
205 leaves (**Fig. 3A**) including, along with Rubisco (**Fig. 1**), a range of chloroplastic proteins involved
206 in photosynthesis, ATP biosynthesis and mRNA translation (**Supplemental Table S4**). Likewise,
207 nuclear genome-encoded proteins upregulated in leaves upon EV infiltration including PR
208 proteins, Kunitz protease inhibitors and stress-related oxidoreductases (**Supplemental Table S5**),
209 were found at lower levels in M2-expressing leaves (**Fig. 3B**).

210 Venn diagrams were produced, and a principal component analysis (PCA) performed, to
211 visually compare the proteomes of non-infiltrated and infiltrated leaves (**Fig. 4, Fig. 5**). Of the 60
212 most upregulated proteins in EV-infiltrated leaves compared to non-infiltrated leaves, 41 (i.e. 68%)
213 were also upregulated in M2-expressing leaves, including several oxidoreductases, PR proteins
214 (β -glucosidases, chitinases) and ER stress-associated proteins (chaperones, protein disulfide
215 isomerases) (blue circles on **Fig. 4A**). Of the 60 most downregulated proteins in EV-infiltrated
216 leaves, 49 (i.e. 82%) were also downregulated in M2-expressing leaves, including
217 photosynthesis-associated proteins (structural components of photosystem I and II, chlorophyll-
218 binding proteins), protein elongation factors and ATPase complex subunits (red circles on **Fig.**
219 **4A**). By comparison, only 18 proteins were found at higher levels, and 29 proteins at lower levels,
220 in both non-infiltrated and M2-expressing leaves compared to EV-infiltrated leaves (**Fig. 4B**). In
221 line with these figures, a PCA analysis of the 1,255 proteins confidently identified by MS/MS in
222 leaf extracts (**Supplemental Table S1**) revealed strongly divergent proteomes in non-infiltrated
223 and EV-infiltrated leaves, compared to M2-expressing leaves exhibiting a hybrid, intermediate
224 proteome (**Fig. 5**). A closer look at the PCA protein distribution indicated a well-defined separation
225 of the 100 most abundant proteins in non-infiltrated and EV-infiltrated leaves (**Supplemental**
226 **Tables S6 and S7**), unlike the 100 most abundant proteins of EV-infiltrated and M2-expressing
227 leaves (**Supplemental Tables S7 and S8**) showing a significantly matching distribution (**Fig. 5**).
228 Together, these data confirmed the occurrence of a hybrid, intermediate proteome in M2-
229 expressing leaves, determined first by the host plant defense response to agroinfiltration, and
230 then by an attenuating effect of M2 on this response presumably associated with an alteration of
231 pH homeostasis along the cell secretory pathway.

232 **Proteome Alterations in Agroinfiltrated Leaves Are Transcriptionally and Post-** 233 **Transcriptionally Determined**

234 Immunoblotting and reverse transcriptase (RT)-qPCR analyses were conducted to statistically

Philippe V. Jutras et al.

235 confirm the validity of our proteomic inferences and to determine whether proteome changes in
236 leaves upon EV infiltration or M2 ectopic expression were transcriptionally or posttranscriptionally
237 regulated (**Fig. 6, Fig. 7**). In line with the Coomassie blue-stained gels above (**Fig. 1**), immunoblot
238 signals for the large and small subunits of Rubisco were the most intense in non-infiltrated leaf
239 samples and the least intense in EV-infiltrated leaf samples (post-ANOVA LSD, $P < 0.05$) (**Fig. 6A**).
240 Likewise, PR-2 and PR-3 proteins were readily detected in both EV- and M2 vector-infiltrated leaf
241 samples, unlike non-infiltrated leaves showing no detectable signals on nitrocellulose membranes
242 ($P < 0.05$) (**Fig. 6B**). As expected given the well described repressing effects of salicylic acid and
243 microbial challenge on the expression of photosynthesis-associated genes (Shimizu et al., 2007;
244 Sugano et al., 2010), mRNA transcript numbers for the two Rubisco subunits were low in
245 agroinfiltrated leaves compared to non-infiltrated leaves (post-ANOVA LSD, $P < 0.05$) (**Fig. 7A**). As
246 also expected, transcript numbers for different stress-related proteins –including PR-3 and PR-10
247 protein isoforms, ER chaperone-associated protein BIP1 and protein disulfide isomerase PD17–
248 showed increased levels in agroinfiltrated leaves ($P < 0.05$) (**Fig. 7B**).

249 Gene expression trends for up- and downregulated proteins followed a similar path in
250 agroinfiltrated leaves compared to non-infiltrated leaves but could not explain the distinct
251 accumulation patterns observed for some of these proteins in EV- and M2 vector-infiltrated leaves.
252 For instance, mRNA transcript numbers for the two subunits of Rubisco decreased to similar
253 levels in EV- and M2 vector-infiltrated leaves (**Fig. 7A**) but higher levels of both subunits were
254 found in M2-expressing leaves (**Fig. 1, Fig. 6A**). Similarly, transcript numbers for the prominent
255 PR-3 protein endochitinase A (Uniprot accession P08252) were comparable in EV- and M2
256 vector-infiltrated leaves (**Fig. 7B**) but PR-3 protein (including endochitinase A) levels were
257 systematically lower upon M2 expression (**Fig. 6B, Supplemental Table S5**). A closer look at the
258 proteome datasets in fact revealed a general trend for the accumulation of stress-related –
259 including ER stress-associated and PR– proteins in agroinfiltrated leaves, by which the steady-
260 state levels of these proteins in M2-expressing leaves, albeit greater than in non-infiltrated leaves,
261 were only ~20–70% the levels measured in EV-infiltrated leaves (**Table 1**). Overall, these data
262 pointed to the onset of transcriptional and posttranscriptional regulatory events in M2-expressing
263 leaves shaping, together, a defense-oriented proteome globally similar to, but nevertheless
264 distinct from, the proteome of EV-infiltrated leaves.

265 **M2 Channel Expression Influences the Protein Secretion Profile of Agroinfiltrated Leaves**

266 Basic reasons for the attenuation of defense (e.g. PR) protein levels and the establishment of a
267 hybrid proteome in M2-expressing leaves remain to be understood. A first explanation could be

Philippe V. Jutras et al.

268 related to the transcriptional downregulation of ER stress-associated proteins such as the
269 chaperone-associated protein BIP1 or the protein disulfide isomerase PDI7 upon M2 channel
270 expression (**Fig. 7B**), which in turn could have limited the efficiency of secreted protein folding
271 and stability in transfected cells. A complementary explanation would be a general interfering
272 effect of M2 channel activity on secreted protein trafficking and host plant defense responses.
273 Several studies have documented the involvement of endomembrane protein trafficking pathways
274 in plant immune responses (Inada et al., 2014; Wang et al., 2016), instrumental to ensure proper
275 secretion of antimicrobial proteins in the apoplast and a rapid migration of pattern-recognition
276 receptor (PRR) proteins towards the plasma membrane (Ben Khaled et al., 2015). The biological
277 significance of intracellular protein trafficking upon microbial challenge is well illustrated on the
278 plant side by the gene inducing effects of salicylic acid, that not only triggers the expression of
279 defense (e.g. PR) proteins and PRR's (Tateda et al., 2014) but also the expression of secretory
280 pathway-associated proteins including ER-resident chaperones and co-chaperones, protein
281 disulfide isomerases and the ER membrane receptor of signal [peptide] recognition particle (Wang
282 et al., 2005). The importance of protein trafficking on the microbial side is illustrated by the
283 production of protein effectors affecting biochemical functions of the host cell secretory pathway
284 (Mukhtar et al., 2011; Weßling et al., 2014) and by the recently reported hijacking of host cell
285 endocytic pathways by agrobacteria to facilitate the trafficking of their virulence factors (Li and
286 Pan, 2017). Considering the importance of pH homeostasis for secreted proteins (Martinière et
287 al., 2013; Jutras et al., 2018), alteration of the Golgi lumen pH by M2 could here have represented
288 a disturbing factor in transfected cells affecting to some extent the processing, trafficking and/or
289 secretion of PRR's and PR proteins following agroinfiltration.

290 We characterized soluble protein profiles in the apoplast of non-infiltrated, EV-infiltrated and
291 M2-expressing leaves to document the eventual impact of M2 on protein secretion (**Fig. 8**).
292 Agroinfiltration was shown previously to trigger a strong upregulation of defense protein secretion
293 in *N. benthamiana* leaves leading to a significant, 4-fold increase of soluble protein content in the
294 apoplast (Goulet et al., 2010b). Accordingly, leaf agroinfiltration increased soluble protein content
295 by 4- to 6-fold in the apoplast, from a baseline content of 0.10 mg protein.ml⁻¹ in apoplast extracts
296 of non-infiltrated leaves to mean contents of 0.40 to 0.56 mg.ml⁻¹ in the extracts of agroinfiltrated
297 leaves (ANOVA; *P*=0.023). Increased apoplastic protein content upon agrobacterial challenge was
298 associated with the secretion of ~28-kDa and 34-kDa proteins (**Fig. 8A**) corresponding to the
299 proteins of similar size immunodetected above with anti-PR-3 (endochitinase A) and anti-PR-2
300 protein antibodies (**Fig. 6B**). In line with iTRAQ and immunodetection data (**Fig. 3B, Fig. 6B**), the
301 major band at 34 kDa was found in M2-expressing leaves at levels about half the corresponding

Philippe V. Jutras et al.

302 levels in EV-infiltrated leaves (**Fig. 8B**) despite similar numbers of mRNA transcripts for
303 endochitinase A in leaves under either treatment (**Fig. 7**). A post-transcriptional mitigating effect
304 of M2 on protein release in the apoplast was further substantiated with GFP variant pHluorin as
305 a recombinant protein model (**Fig. 8C**). We recently reported a positive effect of M2 on pHluorin
306 accumulation in *N. benthamiana* leaves, by which the fluorescence emission rates and steady-
307 state levels of this protein are increased by more than twofold in M2-expressing leaf tissue for a
308 comparable level of pHluorin-encoding transcripts (Jutras et al., 2018). Total pHluorin content in
309 leaf tissue—as inferred from fluorescence emission rates—was here also increased by more than
310 twofold upon M2 expression, but pHluorin content in the apoplast was identical in leaves
311 expressing this protein either alone or along with the viral channel. Together, these observations
312 pointed to a posttranscriptional effect of M2 on host leaf cells altering to some extent the integrity,
313 trafficking and/or secretion of endogenous (e.g. defense) and heterologous proteins during their
314 migration towards the apoplast. A basic question from this point will be to find out where, in the
315 secretory pathway, is M2 influencing the fate of secreted proteins. A practical question will be to
316 determine the resulting output of these effects on the quality and yield of clinically-useful
317 recombinant proteins targeted to the apoplast for proper processing and maturation.

318 **CONCLUSION**

319 Our goal in this study was to look at the impact of influenza virus M2 proton channel expression
320 on the proteome of agroinfiltrated *N. benthamiana* leaves, in an attempt to characterize the
321 possible off-target effects of this accessory protein in a foreign protein production context. M2
322 channel expression was shown recently to trigger a partial neutralization of the Golgi lumen in *N.*
323 *benthamiana* leaf cells helpful to stabilize pH-labile and protease-susceptible recombinant
324 proteins in the cell secretory pathway (Jutras et al., 2015; 2018). We here followed a iTRAQ
325 proteomics procedure to monitor proteome changes in M2-expressing leaves, keeping in mind
326 the involvement of protein secretion in plant cells upon microbial challenge and the importance of
327 pH homeostasis on protein maturation and trafficking in the secretory pathway. Our data pointed
328 overall to a defense response-attenuating effect of M2 upon agroinfiltration, correlated with a
329 restoration of Rubisco and soluble protein contents in leaf tissue. Studies will be welcome in
330 coming years to assess the net impact of M2-induced proteome changes on recombinant protein
331 yields *in planta*. The positive impact of M2 on the production of primary metabolism-associated
332 proteins would suggest in practice an enhanced ability of the plant to accumulate recombinant
333 proteins. The attenuation of defense protein secretion upon M2 expression could indicate by
334 contrast an altered interaction between transfected leaf cells and the bacterial transgene vector

Philippe V. Jutras et al.

335 compromising the ability of the host plant to efficiently process and secrete certain proteins of
336 clinical interest. Work is underway to address these questions using recombinant protein models
337 targeted to different cellular locations. Work is also underway to further assess the impact of M2
338 expression on secreted protein stability and integrity, given the influence of pH on endogenous
339 protease activities in leaves (Jutras et al., 2018) and the possible retrofeedback effects of
340 protease activity alterations on the leaf proteome (Badri et al., 2009; Goulet et al., 2010a).

341 **MATERIALS AND METHODS**

342 **Transgene Constructs**

343 Transgene constructs for pHluorin, M2 proton channel and M2 inactive mutant ^{A30P}M2 were used
344 as described previously (Jutras et al., 2015). Constructs harbored the appropriate DNA coding
345 sequences fused to an upstream N-terminal signal peptide-encoding sequence for co-
346 translational integration of the protein in the cell secretory pathway. The resulting coding
347 sequences were assembled in a pCambia 2300 expression vector harboring an expression
348 cassette for the silencing suppressor protein p19 (CAMBIA), between a duplicated Cauliflower
349 mosaic virus 35S promoter in 5' position and a nopaline synthase terminator sequence in 3'
350 position. An 'empty', pCambia 2300 vector was used as a positive control for the leaf
351 agroinfiltrations. All vectors were maintained in *Agrobacterium tumefaciens*, strain AGL1 (Lazo et
352 al., 1991) until use for the agroinfiltrations.

353 **Transient Expression in Leaves**

354 Bacterial cultures for leaf infiltration were grown to stable phase in Luria-Bertani medium
355 supplemented with appropriate antibiotics, and then harvested by gentle centrifugation at 4,000
356 g for 5 min at 20°C. The bacterial pellets were resuspended in 10 mM MES (2-[N-
357 morpholino]ethanesulfonic acid), pH 5.6, containing 10 mM MgCl₂ to an OD₆₀₀ of 0.5, and
358 incubated for 2 to 4 h at 20°C. Bacterial cultures harboring the M2-encoding vector, the ^{A30P}M2-
359 encoding vector or the empty vector were mixed at a volumic ratio of 1 in 4 with an EV- (or pHluorin
360 vector)-harboring culture grown at the same optical density. The third leaves of 42 d-old plants
361 (down from the main stem apex) were pressure-infiltrated with the bacterial suspensions using a
362 needle-free syringe (D'Aoust et al., 2009), prior to plant incubation at 20°C in a Conviron PWG36
363 growth chamber (Conviron) for heterologous protein expression. Non-infiltrated plants were
364 grown in parallel under the same conditions and used as negative controls. Leaf tissue was
365 harvested 6 d post-infiltration for protein extraction and analysis. Three independent replicates

Philippe V. Jutras et al.

366 each including the third leaf of three plants were used for each treatment to minimize variation of
367 protein expression levels and to allow for statistical analysis of the data (Robert et al., 2013).

368 **Protein Extraction**

369 Leaf tissue for whole-cell protein extraction was harvested as leaf discs representing 160 mg of
370 infiltrated tissue and homogenized by disruption with ceramic beads (BioSpec) in a Mini-Bead
371 beater apparatus (OMNI International). Total soluble proteins were extracted in three volumes of
372 phosphate-buffered saline (PBS), pH 7.3, containing 5 mM EDTA, 0.5% w/v sodium deoxycholate
373 (DOC) and 1 mM phenylmethylsulfonyl fluoride (Sigma-Aldrich). Leaf lysates were clarified by
374 centrifugation for 20 min at 20,000 *g*, and total soluble proteins assayed according to Bradford
375 (1976) with bovine serum albumin as a protein standard (Sigma-Aldrich). The resulting extracts
376 were used directly for SDS-PAGE and immunoblotting, or stored at -20°C to reduce Rubisco
377 levels before proteomic analysis (Qiu et al., 2008; Sainsbury et al., 2016). Leaf apoplast proteins
378 were recovered as described (Robert et al., 2013), with some modifications. Freshly harvested
379 leaves were washed in double-distilled water and submerged in agroinfiltration buffer (10 mM
380 MES buffer, pH 5.8). Washed leaves were vacuum-infiltrated for 60 s at -80 kPa with infiltration
381 buffer, dried off to remove excess buffer, rolled in a homemade Swiss-roll cylinder, and
382 centrifuged at 4°C for 10 min at 1,000 *g* to collect the vacuum infiltrate. The resulting protein
383 preparations were centrifuged at 6,000 *g* for 5 min at 4°C to discard *A. tumefaciens* cells. Protein
384 content was assayed according to Bradford (1976) with bovine serum albumin as a protein
385 standard, and the samples kept at -80°C until further use.

386 **iTRAQ Sample Preparation and Labeling**

387 Whole-cell protein extracts (see above) from three biological replicates were used for iTRAQ
388 proteomics. Similar volumes of the three replicates were pooled and the resulting mixture
389 incubated overnight at -20°C in five volumes of pre-chilled acetone. Precipitated proteins were
390 centrifuged at 20°C for 15 min at 16,000 *g*, and the protein pellets resuspended in 0.5 M
391 triethylammonium bicarbonate (TEAB)–0.5% w/v sodium deoxycholate (DOC) following air drying
392 at 20°C . Protein concentration in each sample was determined according to Bradford (1976), and
393 50 μg of protein was taken apart for iTRAQ labeling. TEAB and DOC were added to the samples
394 at final concentrations of 0.5 M and 0.5% w/v, respectively. The proteins were reduced with Tris(2-
395 carboxyethyl)phosphine (TCEP) and alkylated with methyl methanethiosulfonate (MMTS)
396 according to the iTRAQ kit manufacturer's instructions (Applied Biosystems), and then digested
397 overnight at 37°C with sequence grade-trypsin (Promega) at a protease–protein ratio of 1:30. The

Philippe V. Jutras et al.

398 resulting peptides were acidified to precipitate the DOC detergent, purified with an Oasis HLB
399 cartridge (1 cc, 10 mg; Waters), SpeedVac-dried and dissolved in 30 μ l of 0.5 M TEAB. Four-plex
400 labeling was performed for 2 h in the dark at 20°C with the iTRAQ reagent (Applied Biosystems),
401 and the labeled peptides combined in a single tube. The samples were SpeedVac-dried, cleaned
402 up using an HLB cartridge (Waters) and separated in 14 fractions on a high pH (pH 10) reversed-
403 phase chromatography column using the Agilent 1200 HPLC system (Agilent). Peptide fractions
404 were SpeedVac-dried and resuspended in 0.1% v/v formic acid prior to MS/MS analysis.

405 **Mass Spectrometry**

406 Peptide fractions containing approximately 900 ng of peptides were separated by online reversed-
407 phase nanoscale capillary LC and analyzed by electrospray mass spectrometry. Separations
408 were performed using a Dionex UltiMate 3000 nanoRSLC chromatography system (Thermo
409 Fisher Scientific/Dionex Softron GmbH) connected to an Orbitrap Fusion mass spectrometer
410 (Thermo Scientific) equipped with a nanoelectrospray ion source. The peptides were trapped in
411 loading solvent (2% v/v acetonitrile, 0.05% v/v trifluoroacetic acid) for 5 min at 20 μ L.min⁻¹ on a 5
412 mm x 300 μ m C18 pepmap cartridge pre-column (Thermo Fisher Scientific/Dionex Softron GmbH).
413 The pre-column was switched online to a self-made 50 cm x 75 μ m internal diameter separation
414 column packed with ReproSil-Pur C18-AQ 3- μ m resin (Dr. Maisch HPLC GmbH). The peptides
415 were eluted over 90 min at 300 nL.min⁻¹ along a 5–40% linear gradient of solvent B (80% v/v
416 acetonitrile, 0.1% v/v formic acid) against 0,1% v/v formic acid (solvent A). Mass spectra were
417 acquired under a data-dependent acquisition mode using the Thermo XCalibur software, v. 3.0.63.
418 Full scan mass spectra in the 350–1800 *m/z* range were acquired in the Orbitrap spectrometer
419 using an AGC target of 4e5, a maximum injection time of 50 ms, a resolution of 120,000 and an
420 internal lock mass calibration on *m/z* 445.12003 (siloxane ion). Each MS scan was followed by
421 acquisition of fragmentation MS/MS spectra of the most intense ions for a total cycle time of 3 s
422 (top speed mode). Selected ions were isolated using a quadrupole analyzer in a window of 1.6
423 *m/z*, and fragmented by higher energy collision-induced dissociation with collision energy set at
424 45. Resulting fragments were detected in the Orbitrap at a resolution of 60,000, with an AGC
425 target of 1e5 and a maximum injection time of 120 ms. Dynamic exclusion of previously
426 fragmented peptides was set at a tolerance of 10 ppm for a period of 20 s.

427 **Database Searching**

428 MS/MS spectra were analyzed with the Proteome Discover program, v. 2.1 (Thermo Scientific)
429 set up to search the Solanaceae protein database of Uniprot

Philippe V. Jutras et al.

430 (<http://www.uniprot.org/taxonomy/4070>; 117,836 proteins). Search parameters for matching were
431 as follows: MMTS-alkylated Cys residues and iTRAQ-modified Lys, Tyr and peptide N-terminus
432 as static modifications; oxidized Met residues and deamidated Asn and Gln residues as variable
433 modifications; a mass search tolerance of 10 ppm for MS or 25 atomic mass units for MS/MS;
434 and a maximum of two missed trypsin cleavages allowed. Protein identifications were deemed as
435 valid when a False Discovery Rate of 1% was determined at the peptide and protein levels based
436 on the target-decoy approach (Elias and Gygi, 2007). Protein Discoverer outputs were exported
437 to the Microsoft Excel spreadsheet software, v. 2016 (Microsoft Inc.) for further analysis. A protein
438 was considered as underexpressed when a ratio value of 0.5, or lower than 0.5, was calculated
439 compared to the control; or as overexpressed when this ratio was equal to, or higher than, 2.0.

440 **BLAST Searches and GO Enrichment Analyses**

441 The BLAST (<https://blast.ncbi.nlm.nih.gov/Blast.cgi>) and Blast2GO (<https://www.blast2go.com>)
442 (Conesa et al., 2005) programs were used online to identify and classify the most downregulated,
443 and most upregulated, proteins in leaves under the different experimental treatments. GO
444 enrichment analyses were undertaken to compare the tested proteomes, based on the Gene
445 Ontology system for gene and gene product classification (The Gene Ontology Consortium, 2008).
446 A minimal E-value of 1 was set in Blast2GO for the BLASTP analysis, and the first 20 BLAST hits
447 were selected for further analysis. A number of genes with no annotations in the custom database
448 were annotated, wherever possible, using the GenBank UniProt database
449 (<http://www.uniprot.org>). Predicted subcellular localization of the identified proteins was inferred
450 using the Plant mPloc web server (<http://www.csbio.sjtu.edu.cn/bioinf/plant-multi>) (Chou and
451 Shen, 2010). All DNA sequences were BLAST-searched against the *N. benthamiana* chloroplast
452 genome (<http://sefapps02.qut.edu.au>) to identify chloroplastic proteins.

453 **Principal Component Analysis**

454 A PCA was performed for the proteins confidently identified by MS/MS in protein extracts of non-
455 infiltrated, EV-infiltrated and M2 channel-expressing leaves (i.e. 1,255 proteins overall). The
456 relative abundance of each protein in each group was inferred from the iTRAQ MS/MS dataset
457 (**Supplemental Table S1**). The PCA was performed on log-normalized data using the R software,
458 v. 1.1.423 (R-Studio, www.rstudio.com). Graphical visualization of the PCA data was generated
459 with the *ggbiplot* package.

460 **Immunoblotting and Protein Quantitation by Densitometry**

Philippe V. Jutras et al.

461 Rubisco large (RbcL) and small (RbcS) subunits, PR-2 proteins and PR-3 proteins were detected
462 by immunoblotting on nitrocellulose sheets following 12% (w/v) SDS-PAGE in reducing conditions.
463 Rubisco subunits were detected with polyclonal IgG raised in rabbits against RbcL (Agrisera, Prod.
464 No. AS03 037) or RbcS (AS07 259A). The PR proteins were detected with rabbit polyclonal IgG
465 directed against PR-2 proteins (Agrisera, Prod. No. AS12 2366) or PR-3 proteins (no. AS07 207).
466 Nonspecific binding on nitrocellulose sheets was prevented by incubation in blocking solution (5%
467 w/v skim milk powder in PBS, containing 0.025% v/v Tween-20), which also served as antibody
468 dilution buffer. The primary antibodies were detected with goat anti-rabbit secondary antibodies
469 conjugated to alkaline phosphatase (Sigma-Aldrich). Protein signals were developed with the
470 alkaline phosphatase substrate 5-bromo-4-chloro-3-indolyl phosphate and nitro blue tetrazolium
471 as a colour indicator (Life Technologies). Densitometric analysis was performed using the
472 Phoretix 2D Expression software v. 2005 (NonLinear USA) on non-saturated immunoblot images
473 digitalized with an Amersham Image Scanner (GE Healthcare). All measurements were made
474 with leaf extracts from at least three independent (plant) replicates.

475 **RNA Extraction and Quantification of mRNA Transcripts**

476 RT-qPCR assays were performed with leaf samples from four plant replicates each harvested as
477 two leaf discs representing 100 mg of fresh tissue. Leaf discs were ground in liquid nitrogen and
478 total RNA extracted using the EZ-10 Spin Column Plant RNA Miniprep Kit (Biobasics). Residual
479 DNA was removed using the RNase-free DNase Set (Qiagen) and RNA integrity assessed using
480 an Agilent 2100 Bioanalyzer (Agilent Technologies). RNA quality was confirmed and
481 concentration determined using a NanoDrop ND-1000 spectrophotometer (NanoDrop
482 Technologies, Wilmington DE, U.S.A.), before reverse transcription to cDNA using the QuantiTect
483 Reverse Transcription kit (Qiagen). Transcript quantification was performed by real-time RT-
484 qPCR in 96-well plates using the ABI PRISM 7500 Fast real-time PCR system and custom data
485 analysis software, version 2.0.1 (Thermo Fisher Scientific). Each PCR reaction contained 5 ng of
486 cDNA template, 0.5 μ M forward and reverse primers for target gene amplification (**Supplemental**
487 **Table 9**) and 1X SYBR Green Master Mix (QuantiTect SYBR Green mix, Qiagen), for a total
488 volume of 10 μ L. qPCR was run under the SYBR Green amplification mode at the following PCR
489 cycling conditions: 15 min incubation at 95°C, followed by 40 amplification cycles at 95°C for 5 s,
490 60°C for 30 s, and 65°C for 90 s. Reactions in the absence of cDNA template were conducted as
491 negative controls and fluorescence readings were taken at the end of each cycle. The absence
492 of DNA primer dimers and specificity of the amplifications were confirmed by melting curve
493 analysis at the end of each reaction. Fluorescence and cycle threshold (Ct) values were exported

Philippe V. Jutras et al.

494 to and analyzed using the Microsoft Excel spreadsheet software, v. 2016 (Microsoft, Inc.). The
495 relative number of transcripts ($1/2^{Ct}$) was averaged from technical RT-qPCR duplicates and used
496 for subsequent normalization. Expression data were normalized against the geometric mean of
497 six reference genes (**Supplemental Table S9**) to correct for biological variability and technical
498 variations during RNA extraction, quantification and reverse transcription. Stability of reference
499 gene expression was evaluated using the geNORM VBA applet for Microsoft Excel
500 (Vandesompele et al., 2002). Fold changes in gene expression, reported relative to EV-infiltrated
501 leaf tissue, were calculated using the $2^{-\Delta\Delta Ct}$ method (Livak and Schmittgen, 2001; Bustin et al.,
502 2009). Standard deviation (SD) related to within-treatment biological variation was calculated in
503 accordance with the error propagation rules.

504 **Recombinant pFluorin Quantification**

505 pFluorin expression was monitored by detection of fluorescence emission with a Fluostar Galaxy
506 microplate reader (BMG, Offenburg, Germany) using excitation and emission filters of 485 and
507 520 nm, respectively (Jutras et al., 2018). Fluorescence levels were expressed relative to
508 fluorescence emission in M2-free (– M2) ‘control’ extracts. Samples were loaded in triplicate on
509 Costar 96-well black polystyrene plates (Cedarlane, Burlington ON, Canada). All measurements
510 were made with leaf protein extracts from six independent (plant) replicates.

511 **Statistical Analyses**

512 Statistical analyses were performed using RStudio, v. 0.98.1103 (RStudio, Inc.). Analysis of
513 variance (ANOVA) tests were used to compare peptide (protein) counts and mRNA transcript
514 numbers among treatments. Contrast calculations and LSD mean comparison tests were
515 performed for those ANOVA giving significant *P* values at an alpha value threshold of 5%.

516 **Supplemental Data**

517 **Fig. S1** Complement to Fig. 1: Soluble protein content over 12 d in non-infiltrated leaves or
518 agroinfiltrated leaves expressing or not the M2 proton channel

519 **Fig. S2** Complement to Fig. 2: GO enrichment analysis of iTRAQ-quantified proteins up- or
520 downregulated in EV-infiltrated leaves compared to non-infiltrated control leaves

521 **Fig. S3** Complement to Fig. 3: GO enrichment analysis of iTRAQ-quantified proteins up- or
522 downregulated in M2 vector-infiltrated leaves compared to EV-infiltrated leaves

523 **Table S1** Complete list of confidently identified proteins following iTRAQ analysis

Philippe V. Jutras et al.

- 524 **Table S2** The 60 most upregulated proteins in EV-infiltrated leaves compared to non-infiltrated
525 control leaves
- 526 **Table S3** The 60 most downregulated proteins in EV-infiltrated leaves compared to non-
527 infiltrated control leaves
- 528 **Table S4** The 60 most upregulated proteins in M2 vector-infiltrated leaves compared to EV-
529 infiltrated leaves
- 530 **Table S5** The 60 most downregulated proteins in M2 vector-infiltrated leaves compared to EV-
531 infiltrated leaves
- 532 **Table S6** The 100 most abundant proteins in non-infiltrated leaves
- 533 **Table S7** The 100 most abundant proteins in EV-infiltrated leaves
- 534 **Table S8** The 100 most abundant proteins in M2-channel expressing leaves
- 535 **Table S9** DNA primers for RT-qPCR amplifications

536 **ACKNOWLEDGMENTS**

537 This work was supported by a Discovery grant from the Natural Science and Engineering
538 Research Council (NSERC) of Canada to D.M. P.V.J. was the recipient of an AgroPhytoSciences
539 NSERC–CREATE scholarship and of a BMP graduate scholarship co-funded by Medicago inc.,
540 NSERC and Québec Government’s research funding body FRQNT.

541 **LITERATURE CITED**

- 542 **Anand A, Uppalapati SR, Ryu CM, Allen SN, Kang L, Tang Y, Musore KS** (2008) Salicylic acid
543 and systemic acquired resistance play a role in attenuating Crown gall disease caused by
544 *Agrobacterium tumefaciens*. *Plant Physiol* **146**: 703–715
- 545 **Ashnest JR, Huynh DL, Dragwidge JM, Ford BA, Gendall AR** (2015) Arabidopsis intracellular
546 NHX-type sodium-proton antiporters are required for seed storage protein processing. *Plant*
547 *Cell Physiol* **56**: 2220–2233
- 548 **Badri MA, Rivard D, Coenen K, Michaud D** (2009) Unintended molecular interactions in
549 transgenic plants expressing clinically-useful proteins–The case of bovine aprotinin travelling
550 the potato leaf cell secretory pathway. *Proteomics* **9**: 746–756
- 551 **Bassil E, Blumwald E** (2014) The ins and outs of intracellular ion homeostasis: NHX-type
552 cation/H⁺ transporters. *Curr Opin Plant Biol* **22**: 1–6

Philippe V. Jutras et al.

- 553 **Ben Khaled S, Robatzek S** (2015) A moving view: subcellular trafficking processes in pattern
554 recognition receptor-triggered plant immunity. *Annu Rev Plant Biol* **53**: 379–402
- 555 **Boller T, Felix G** (2009) A renaissance of elicitors: perception of microbe-associated molecular
556 patterns and danger signals by pattern recognition receptors. *Annu Rev Plant Biol* **60**: 379–
557 406
- 558 **Bradford MM** (1976) A rapid and sensitive method for the quantitation of microgram quantities of
559 protein utilizing the principle of protein-dye binding. *Anal Biochem* **72**: 248–254
- 560 **Brewis IA, Brennan P** (2010) Proteomics technologies for the global identification and
561 quantification of proteins. *Adv Prot Chem Struct Biol* **80**: 1–43
- 562 **Bustin SA, Benes V, Garson JA, Hellems J, Huggett J, Kubista M, Mueller R, Nolan T,
563 Pfaffl MW, Shipley GL, et al.** (2009) The MIQE guidelines: minimum information for
564 publication of quantitative realtime PCR experiments. *Clin Chem* **55**: 611–622
- 565 **Cady SD, Luo W, Hu F, Hong M** (2009) Structure and function of the Influenza A M2 proton
566 channel. *Biochemistry* **48**: 7356–7364
- 567 **Chou KC, Shen HB** (2010) Plant-mPLoc: A top-down strategy to augment the power for
568 predicting plant protein subcellular localization. *PLoS One* **5**: e11335
- 569 **Conesa A, Götz S, García-Gómez JM, Terol J, Talón M, Robles M** (2005) Blast2GO: a
570 universal tool for annotation, visualization and analysis in functional genomics research.
571 *Bioinformatics* **21**: 3674–3676
- 572 **D'Aoust MA, Lavoie PO, Belles-Iles J, Bechtold N, Martel M, Vézina LP** (2009) Transient
573 expression of antibodies in plants using syringe agroinfiltration. *Meth Mol Biol* **483**: 41–50
- 574 **Dettmer J, Hong-Hermesdorf A, Stierhof YD, Schumacher K** (2006) Vacuolar H⁺-ATPase
575 activity is required for endocytic and secretory trafficking in *Arabidopsis*. *Plant Cell* **18**: 715–
576 730
- 577 **Elias JE, Gygi SP** (2007) Target-decoy search strategy for increased confidence in large-scale
578 protein identifications by mass spectrometry. *Nat Meth* **4**: 207–214
- 579 **Faye L, Boulafloous A, Benchabane M, Gomord V, Michaud D** (2005) Protein modifications in
580 the plant secretory pathway: current status and practical implications in molecular pharming.
581 *Vaccine* **23**: 1770–1778
- 582 **Gomord V, Fichette AC, Menu-Bouaouiche L, Saint-Jore-Dupas C, Plasson C, Michaud D,**

Philippe V. Jutras et al.

- 583 **Faye L** (2010) Plant-specific glycosylation patterns in the context of therapeutic protein
584 production. *Plant Biotechnol J* **8**: 564–587
- 585 **Goulet C, Khalf M, Sainsbury F, D’Aoust MA, Michaud D** (2012) A protease activity-depleted
586 environment for heterologous proteins migrating towards the leaf cell apoplast. *Plant*
587 *Biotechnol J* **10**: 83–94
- 588 **Goulet C, Benchabane M, Anguenot R, Brunelle F, Khalf M, Michaud D** (2010a) A companion
589 protease inhibitor for the protection of cytosol-targeted recombinant proteins in plants. *Plant*
590 *Biotechnol J* **8**: 142–154
- 591 **Goulet C, Goulet C, Goulet MC, Michaud D** (2010b) 2-DE proteome maps for the leaf apoplast
592 of *Nicotiana benthamiana*. *Proteomics* **10**: 2536–2544
- 593 **Henkel JR, Weisz OA** (1998) Influenza virus M2 protein slows traffic along the secretory
594 pathway. pH perturbation of acidified compartments affects early Golgi transport steps. *J Biol*
595 *Chem* **273**: 6518–6524
- 596 **Holsinger LJ, Nichani D, Pinto LH, Lamb RA** (1994) Influenza A virus M2 ion channel protein:
597 a structure-function analysis. *J Virol* **68**: 1551–1563
- 598 **Ishiga Y, Watanabe M, Ishiga T, Tohge T, Matsuura T, Ikeda Y, Hoefgen R, Fernie AR,**
599 **Mysore KS** (2017) The SAL-PAP chloroplast retrograde pathway contributes to plant immunity
600 by regulating glucosinolate pathway and phytohormone signaling. *Mol Plant–Microbe Interact*
601 **30**: 829–841
- 602 **Inada N, Ueda T** (2014) Membrane trafficking pathways and their roles in plant–microbe
603 interactions. *Plant Cell Physiol* **55**: 672–686
- 604 **Jutras PV, Goulet MC, Lavoie PO, D’Aoust MA, Sainsbury F, Michaud D** (2018) Recombinant
605 protein susceptibility to proteolysis in the plant cell secretory pathway is pH-dependent. *Plant*
606 *Biotechnol J* (in press): doi.org/10.1111/pbi.12928.
- 607 **Jutras PV, Marusic C, Lonoce C, Deflers C, Goulet MC, Benvenuto E, Michaud D, Donini M**
608 (2016) An accessory protease inhibitor to increase the yield and quality of a tumour-targeting
609 mAb in *Nicotiana benthamiana* leaves. *PLoS One* **11**, e0167086
- 610 **Jutras PV, D’Aoust MAA, Couture MMJ, Vézina LP, Goulet MC, Michaud D, Sainsbury F**
611 (2015) Modulating secretory pathway pH by proton channel co-expression can increase
612 recombinant protein stability in plants. *Biotechnol J* **10**: 1478–1486

Philippe V. Jutras et al.

- 613 **Lazo GR, Stein PA, Ludwig RA** (1991) A DNA transformation-competent *Arabidopsis* genomic
614 library in *Agrobacterium*. *Biotechnology* **9**: 963–967
- 615 **Li X, Pan SQ** (2017) *Agrobacterium* delivers VirE2 protein into host cells via clathrin-mediated
616 endocytosis. *Sci Adv* **3**: e1601528
- 617 **Livak KJ, Schmittgen TD** (2001) Analysis of relative gene expression data using real-time
618 quantitative PCR and the $2^{-\Delta\Delta C(T)}$ method. *Methods* **25**: 402–408
- 619 **Lomonossoff GP, D’Aoust MA** (2016) Plant-produced biopharmaceuticals: A case of technical
620 developments driving clinical deployment. *Science* **353**: 1237–1240
- 621 **Makhzoum A, Benyammi R, Koustafa, K, Trémouillaux-Guiller J** (2014) Recent advances on
622 host plants and expression cassettes’ structure and function in plant molecular pharming.
623 *BioDrugs* **28**: 145–159
- 624 **Mandal MK, Ahvari H, Schillberg S, Schiermeyer A** (2016) Tackling unwanted proteolysis in
625 plant production hosts used for molecular farming. *Front Plant Sci* **7**: 1–6
- 626 **Martinière A, Bassil E, Jublanc E, Alcon C, Reguera M, Sentenac H, Blumwald E, Paris D**
627 (2013) In vivo intracellular pH measurements in tobacco and *Arabidopsis* reveal an unexpected
628 pH gradient in the endomembrane system. *Plant Cell* **25**: 4028–4043
- 629 **Mukhtar MS, Carvunis AR, Dreze M, Epple P, Steinbrenner J, Moore J, Tasan M, Galli M,**
630 **Hao T, Nishimura MT, Pevzner SJ, Donovan SE, Ghamsari L, Santhanam B, Romero V,**
631 **Poulin MM, Gebreab F, Gutierrez BJ, Tam S, Monachello D, Boxem M, Harbort CJ,**
632 **McDonald N, Gai L, Chen H, He Y, European Union Effectoromics Consortium,**
633 **Vandehaute J, Roth FP, Hill DE, Ecker JR, Vidal M, Beynon J, Braun P, Dangl JL** (2011)
634 Independently evolved virulence effectors converge onto hubs in a plant immune system
635 network. *Science* **3111**: 596–601
- 636 **Nagatoshi Y, Ikeda M, Kishi H, Hiratsu K, Muraguchi A, Ohme-Takagi M** (2015) Induction of
637 a dwarf phenotype with IBH1 may enable increased production of plant-made pharmaceuticals
638 in plant factory conditions. *Plant Biotechnol J* **14**: 887–894
- 639 **Nomura H, Komori T, Uemura S, Kanda Y, Shimotani K, Nakai K, Furuichi T, Takebayashi**
640 **K, Sugimoto T, Sano S, Suwastika IN, Fukusaki E, Yoshioka H, Nakahira Y, Shiina T** (2012)
641 Chloroplast-mediated activation of plant immune signalling in *Arabidopsis*. *Nat Commun* **3**: 926
- 642 **Orlowski J, Grinstein S** (2011) Na⁺/H⁺ exchangers. *Comprehensive Physiol* **1**: 2083–2100

Philippe V. Jutras et al.

- 643 **Pillay P, Schlüter U, van Wyk S, Kunert KJ, Vorster BJ** (2014) Proteolysis of recombinant
644 proteins in bioengineered plant cells. *Bioengineered* **5**: 1–6
- 645 **Pruss GJ, Nester EW, Vance V** (2008) Infiltration with *Agrobacterium tumefaciens* induces host
646 defense and development-dependent responses in the infiltrated zone. *Mol Plant-Microbe*
647 *Interact* **21**: 1528–1538
- 648 **Qiu QS, Huber JL, Booker FL, Jain V, Leakey ADB, Fiscus EL, Yau PM, Ort DR, Huber SC**
649 (2008) Increased protein carbonylation in leaves of *Arabidopsis* and soybean in response to
650 elevated [CO₂]. *Photosynth Res* **97**: 155–166
- 651 **Reguera M, Bassil E, Tajima H, Wimmer M, Chanoca A, Otegui MS, Paris N, Blumwald E**
652 (2015) pH regulation by NHX-type antiporters is required for receptor-mediated protein
653 trafficking to the vacuole in *Arabidopsis*. *Plant Cell* **27**: 1200–1217
- 654 **Robert S, Jutras PV, Khalf M, D’Aoust MA, Goulet MC, Sainsbury F, Michaud D** (2016)
655 Companion protease inhibitors for the *in situ* protection of recombinant proteins in plants. *Meth*
656 *Mol Biol* **1385**: 115–126
- 657 **Robert S, Goulet MC, D’Aoust MA, Sainsbury F, Michaud D** (2015) Leaf proteome rebalancing
658 in *Nicotiana benthamiana* for upstream enrichment of a transiently expressed recombinant
659 protein. *Plant Biotechnol J* **13**: 1169–1179
- 660 **Robert S, Khalf M, Goulet MC, D’Aoust MA, Sainsbury F, Michaud D** (2013) Protection of
661 recombinant mammalian antibodies from development-dependent proteolysis in leaves of
662 *Nicotiana benthamiana*. *PLoS One* **8**: e70203
- 663 **Sainsbury F, Jutras PV, Vorster J, Goulet MC, Michaud D** (2016) A chimeric affinity tag for
664 efficient expression and chromatographic purification of heterologous proteins from plants.
665 *Front Plant Sci* **7**: 141
- 666 **Sack M, Hofbauer A, Fischer R, Stoger E** (2015) The increasing value of plant-made proteins.
667 *Curr Opin Biotechnol* **32**: 163–170
- 668 **Sakaguchi T, Leser GP, Lamb RA** (1996) The ion channel activity of the Influenza virus M₂
669 protein affects transport through the Golgi apparatus. *J Cell Biol* **133**: 733–747
- 670 **Schnell JR, Chou JJ** (2008) Structure and mechanism of the M2 proton channel of influenza A
671 virus. *Nature* **451**: 591–595
- 672 **Schumacher K** (2014) pH in the plant endomembrane system—an import and export business.

Philippe V. Jutras et al.

- 673 Curr Opin Plant Biol **22**: 71–76
- 674 **Serrano I, Audran C, Rivas S** (2016) Chloroplasts at work during plant innate immunity. J Exp
675 Bot **67**: 3845–3854
- 676 **Shen J, Zeng Y, Zhuang X, Sun L, Yao X, Pimpl P, Jiang L** (2013) Organelle pH in the
677 *Arabidopsis* endomembrane system. Mol Plant **6**: 1419–1437
- 678 **Shimizu T, Satoh K, Kikuchi S, Omura T** (2007) The repression of cell wall- and plastid-related
679 genes and the induction of defense-related genes in rice plants infected with *Rice dwarf virus*.
680 Mol Plant–Microbe Interact **3**: 247–254
- 681 **Stöger E, Fischer R, Moloney M, Ma JKC** (2014) Plant molecular pharming for the treatment of
682 chronic and infectious diseases. Annu Rev Plant Biol **65**: 743–768
- 683 **Streatfield SJ** (2007) Approaches to achieve high-level heterologous protein production in plants.
684 Plant Biotechnol J **5**: 2–16
- 685 **Sugano S, Jiang CJ, Miyazawa SI, Masumoto C, Yazawa K, Hayashi N, Shimono M,**
686 **Nakayama A, Miyao M, Takatsuji H** (2010) Role of OsNPR1 in rice defense program as
687 revealed by genome-wide expression analysis. Plant Mol Biol **74**: 549–562
- 688 **Takatsuji H** (2017) Regulating tradeoffs to improve rice production. Front Plant Sci **8**: 171
- 689 **Tateda C, Zhang Z, Shrestha J, Jelenska J, Chinchilla D, Greenberg JT** (2014) Salicylic acid
690 regulates *Arabidopsis* microbial pattern receptor kinase levels and signaling. Plant Cell **26**:
691 4171–4187
- 692 **The Gene Ontology Consortium** (2008) The Gene Ontology project in 2008. Nucl Acids Res **36**:
693 D440–444
- 694 **Tschofen M, Knopp D, Hood E, Stöger E** (2016) Plant molecular farming: much more than
695 medicines. Annu Rev Plant Biol **9**: 271–294
- 696 **Vandesompele J, De Preter K, Pattyn F, Poppe B, Van Roy N, De Paepe A, Speleman F**
697 (2002) Accurate normalization of real-time quantitative RT-PCR data by geometric averaging
698 of multiple internal control genes. Genome Biol **3**: 34
- 699 **Wang D, Weaver ND, Kesarwani M, Dong X** (2005) Induction of protein secretory pathway is
700 required for systemic acquired resistance. Science **308**: 1036–1040
- 701 **Wang WM, Liu PQ, Xu YJ, Xiao S** (2016) Protein trafficking during plant innate immunity. J Integr

Philippe V. Jutras et al.

- 702 Plant Biol **58**: 284–298
- 703 **Weßling R, Epple P, Altmann S, He Y, Yang L, Henz SR, McDonald N, Wiley K, Bader KC,**
704 **Gläßer C, Mukhtar MS, Haigis S, Ghamsari L, Stephens AE, Ecker JR, Vidal M, Jones**
705 **JDG, Mayer KFX, Ver Loren van Themaat E, Weigel D, Schulze-Lefert P, Dangl JL,**
706 **Panstruga R, Braun P** (2014) Convergent Targeting of a Common Host Protein-Network by
707 Pathogen Effectors from Three Kingdoms of Life. *Cell Host Micr* **16**: 364–375
- 708 **Wilbers RHP, Westerhof RB, van Raaij DR, van Adrichem M, Prakasa AD, Lozano-Torres**
709 **JL, Bakker J, Smant G, Schots A** (2016) Co-expression of the protease furin in *Nicotiana*
710 *benthamiana* leads to efficient processing of latent transforming growth factor- β 1 into a
711 biologically active protein. *Plant Biotechnol J* **14**: 1695–1704
- 712 **Wu X, Ebine K, Ueda T, Qiu QS** (2016) AtNHX5 and AtNHX6 are required for the subcellular
713 localization of the SNARE complex that mediates the trafficking of seed storage proteins in
714 *Arabidopsis*. *PLoS One* **11**: e0151658
- 715 **Xiao Y, Savchenko T, Bidoo EEK, Chehab WE, Hayden DM, Tolstikov V, Corwin JA,**
716 **Kliebenstein DJ, Keasling JD, Dehesh K** (2012) Retrograde signaling by the plastidial
717 metabolite MEcPP regulates expression of nuclear stress-response genes. *Cell* **149**: 1525–
718 1535

719
 720 **Table 1.** Relative abundance of stress-related proteins in EV-infiltrated [or M2-expressing] leaves compared to non-infiltrated [or EV-
 721 infiltrated] leaves ¹

722

723

724	Accession	Protein family	Protein name	Relative abundance		
725				EV/n.i. ²	M2/n.i.	M2/EV
727	P23432	PR-2	Glucan endo-1,3-beta-glucosidase	21.5	6.9	0.32
728	Q84LQ7	PR-3	29-kDa chitinase-like thermal hysteresis protein	7.4	2.8	0.38
729	P08252	PR-3	Endochitinase A	6.0	2.5	0.42
730	P07052	PR-5	Pathogenesis-related R major form	6.0	1.6	0.27
731	Q50LG4	PR-9	Suberization-associated anionic peroxidase-like	8.9	2.0	0.22
732	J9XUY3	Protease inhibitor	Kunitz-type protease inhibitor	15.2	1.3	0.09
733	DHIHB9	Protease inhibitor	Kunitz-type trypsin inhibitor alpha chain-like	8.2	1.9	0.24
734	A0A0B5GNH2	ER stress	ER chaperone-binding protein	6.6	4.0	0.60
735	K4C2W4	ER stress	Protein disulfide isomerase	6.1	4.3	0.71

736

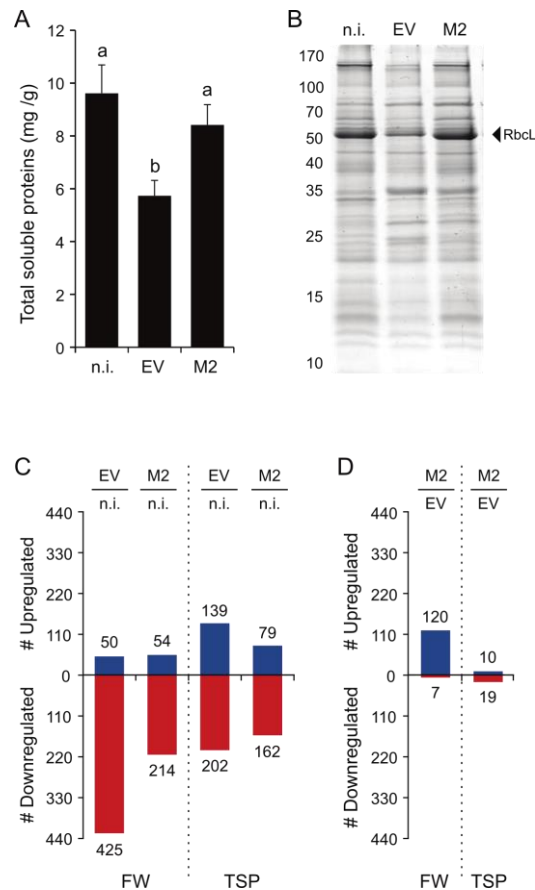
737

738 ¹ Ratios were inferred from MS/MS peptide abundance values determined for each protein under the three treatments
 739 (**Supplemental Table S7**). Data are provided for stress-related proteins up-regulated by at least 5-fold in EV-infiltrated leaves
 740 (**Supplemental Table S2**).

741 ² n.i., non-infiltrated.

742 **FIGURES**

743

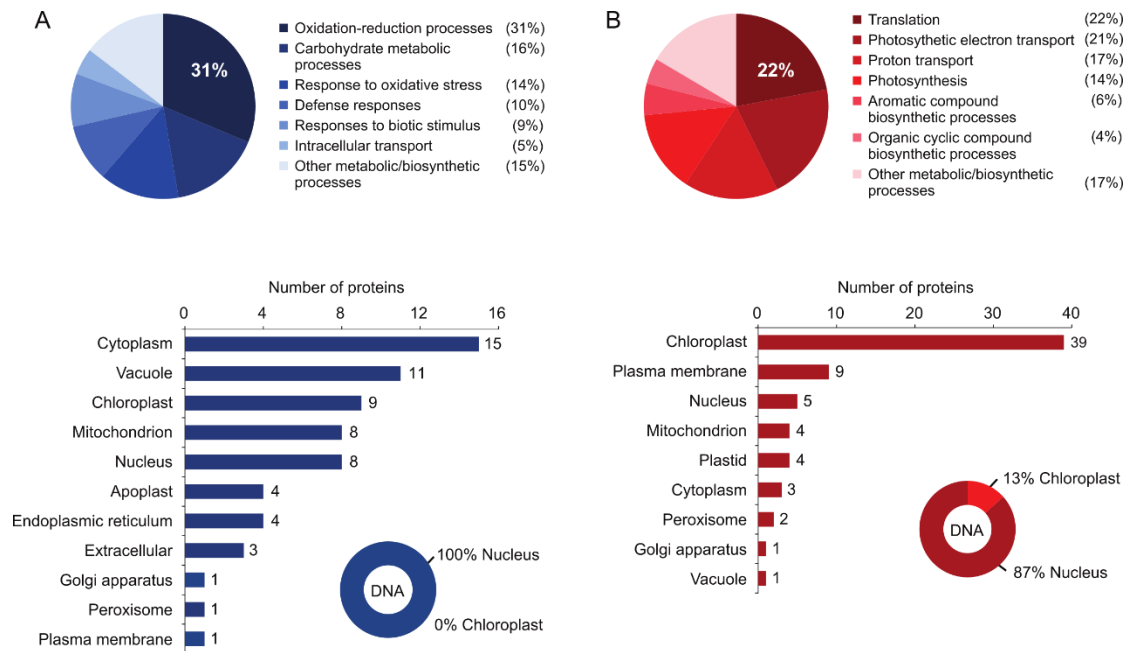


744

745 **Figure 1.** Soluble protein content and proteome changes in non-infiltrated (n.i.), EV-infiltrated and
746 M2 channel-expressing leaves 6 d post-agroinfiltration. (A) Total soluble proteins (TSP) in leaf
747 tissue, as expressed on a leaf fresh weight basis. Data are the mean of three biological (plant)
748 replicate values \pm SD. Bars with the same letter are not significantly different (post-ANOVA LSD;
749 $P < 0.05$). (B) Soluble protein profiles in leaves as observed on Coomassie blue-stained
750 polyacrylamide gels following 12% w/v SDS-PAGE. Numbers on the left refer to commercial
751 molecular weight markers. Arrow on the right points to the large, 52-kDa subunit of Rubisco. (C)
752 Numbers of iTRAQ-identified proteins up- (blue) or down- (red) regulated by at least twofold in
753 EV-infiltrated and M2-expressing leaves compared to non-infiltrated control leaves. (D) Numbers
754 of iTRAQ-identified proteins up (blue) or down- (red) regulated (blue) by at least twofold in M2-
755 expressing leaves compared to EV-infiltrated leaves. Data on panels C and D are expressed on
756 a leaf fresh weight (FW) or protein-specific (TSP) basis. Additional data on leaf soluble protein
757 content are provided in **Supplemental Fig. S1**.

Philippe V. Jutras et al.

758

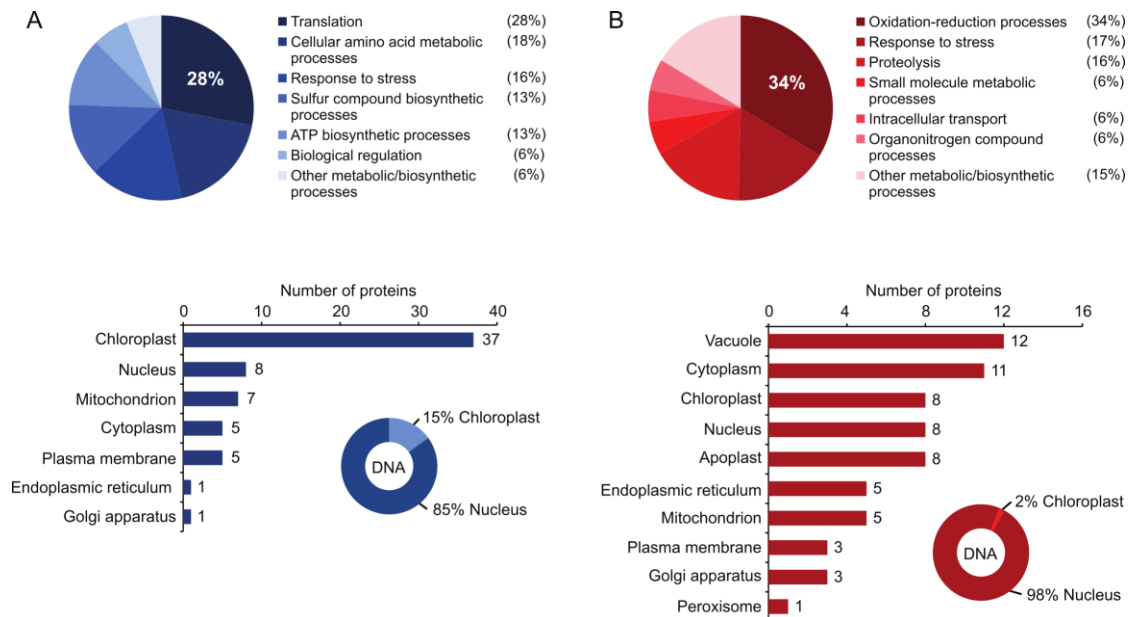


759

760 **Figure 2.** GO enrichment analysis of iTRAQ-quantified proteins up- (A, in blue) or down- (B, in
761 red) regulated by at least twofold in EV-infiltrated leaves compared to non-infiltrated (n.i.) leaves.
762 Pie charts identify the six most affected biological processes in leaves as inferred from biological
763 functions assigned to the 60 most upregulated, or 60 most downregulated, proteins in EV-
764 infiltrated leaves. Bar charts summarize the subcellular distribution of these proteins as inferred
765 *in silico* from their predicted cellular localization. Circle charts indicate the relative abundance of
766 chloroplast genome- and nuclear genome-encoded proteins among these same proteins. The 60
767 most upregulated, and 60 most downregulated, proteins in EV-infiltrated leaves compared to non-
768 infiltrated leaves are listed in **Supplemental Tables S2** and **S3**, respectively. Complementary
769 information to this GO enrichment analysis is provided in **Supplemental Fig. S2**.

Philippe V. Jutras et al.

770



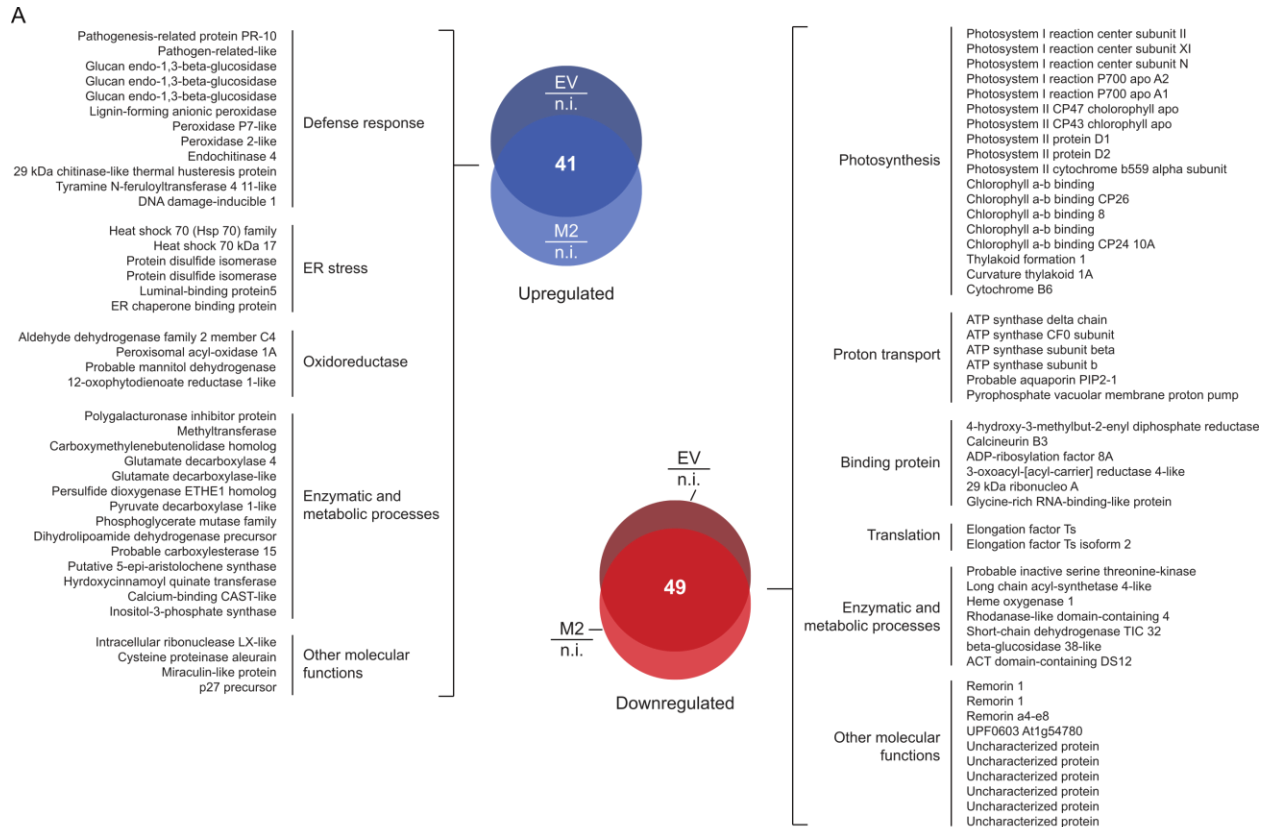
771

772 **Figure 3.** GO enrichment analysis of iTRAQ-quantified proteins up- (A, in blue) or down- (B, in
773 red) regulated by at least twofold in M2 vector-infiltrated leaves compared to EV-infiltrated leaves.
774 Pie charts identify the six most affected biological processes in leaves as inferred from biological
775 functions assigned to the 60 most upregulated, or 60 most downregulated, proteins in M2-
776 expressing leaves. Bar charts summarize the subcellular distribution of these proteins as inferred
777 *in silico* from their predicted cellular localization. Circle charts indicate the relative abundance of
778 chloroplast genome- and nuclear genome-encoded proteins among these same proteins. The 60
779 most upregulated, and 60 most downregulated, proteins in M2-expressing leaves compared to
780 non-infiltrated leaves are listed in **Supplemental Tables S4** and **S5**, respectively. Additional
781 information on this GO enrichment analysis is provided in **Supplemental Fig. S3**.

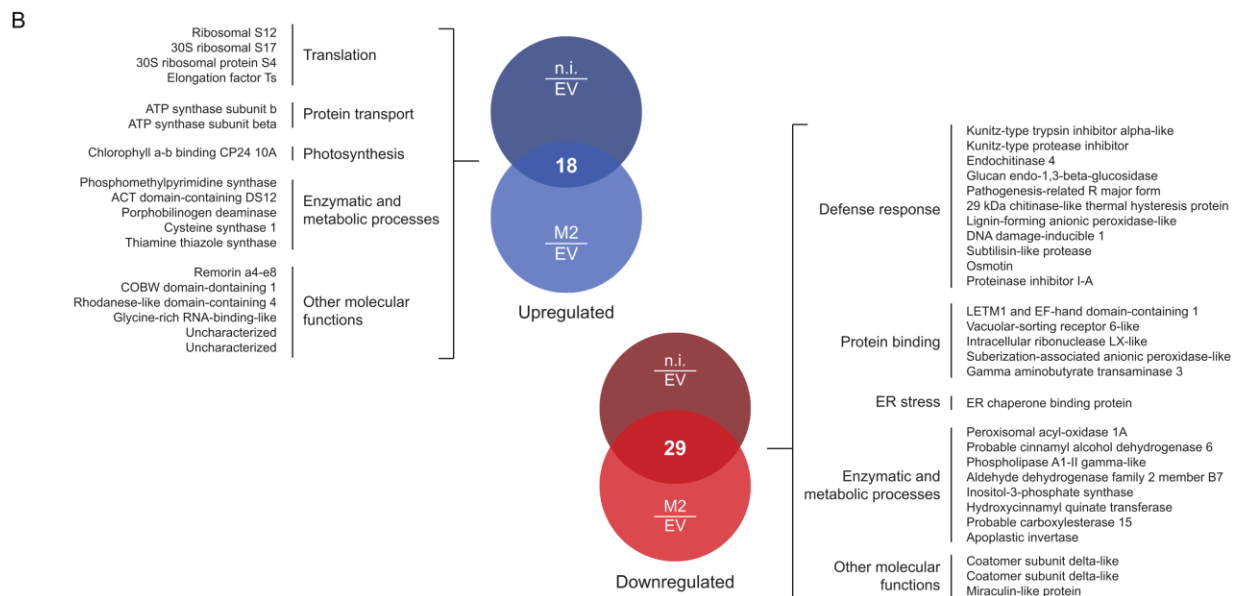
782 **Figure 4.** (next page) Venn diagrams for the proteins up- (blue) and down- (red) regulated in two
783 [test] treatments relative to the third [reference] treatment. (A) Proteins up- or downregulated in
784 EV-infiltrated and M2-expressing leaves compared to non-infiltrated (n.i.) leaves. (B) Proteins up-
785 or downregulated in non-infiltrated and M2-expressing leaves compared to EV-infiltrated leaves.
786 Numbers in overlapping areas indicate the numbers of proteins up- or downregulated in both test
787 treatments compared to the reference treatment, out of the 60 most affected proteins in each test
788 treatment. Protein lists identify those up- (left-hand side) and down- (right-hand side) regulated
789 proteins shared by the two test treatments.

Philippe V. Jutras et al.

790

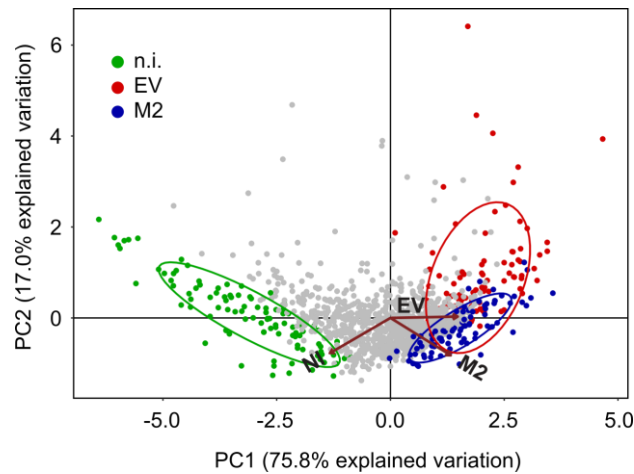


791



Philippe V. Jutras et al.

792

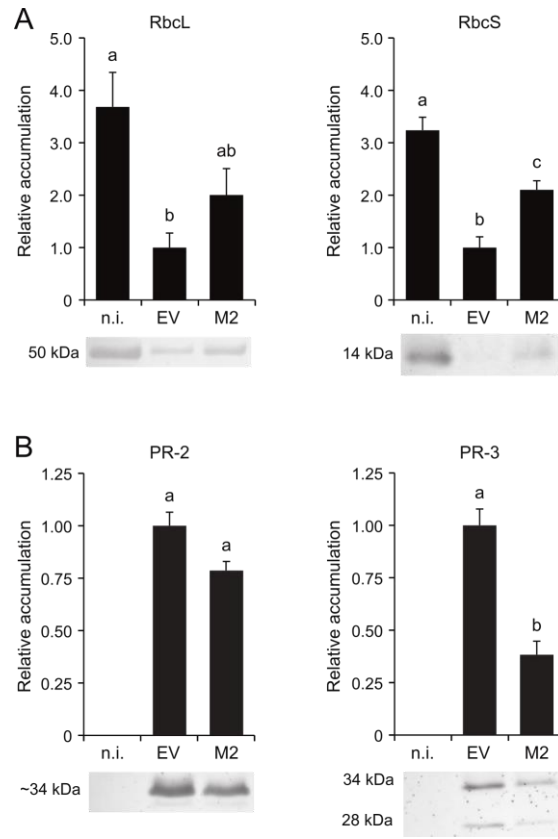


793

794 **Figure 5.** Principal component analysis (PCA) of MS/MS identified proteins in non-infiltrated (n.i.),
795 EV-infiltrated and M2-expressing leaves. The vectors indicate strongly divergent proteomes in
796 non-infiltrated and EV-infiltrated leaves, compared to M2-expressing leaves exhibiting a hybrid
797 proteome matching in part the proteome of EV-infiltrated leaves. The 100 most abundant proteins
798 of each group are coloured to further highlight differences and similarities between non-infiltrated
799 (green), EV-infiltrated (red) and M2-expressing (blue) leaf proteomes. Confidence ellipses show
800 normal data probability for each group of proteins (by default to 68%). The 100 most abundant
801 proteins for either treatments are listed and their relative abundance in leaves given in
802 **Supplemental Tables S6, S7 and S8.**

Philippe V. Jutras et al.

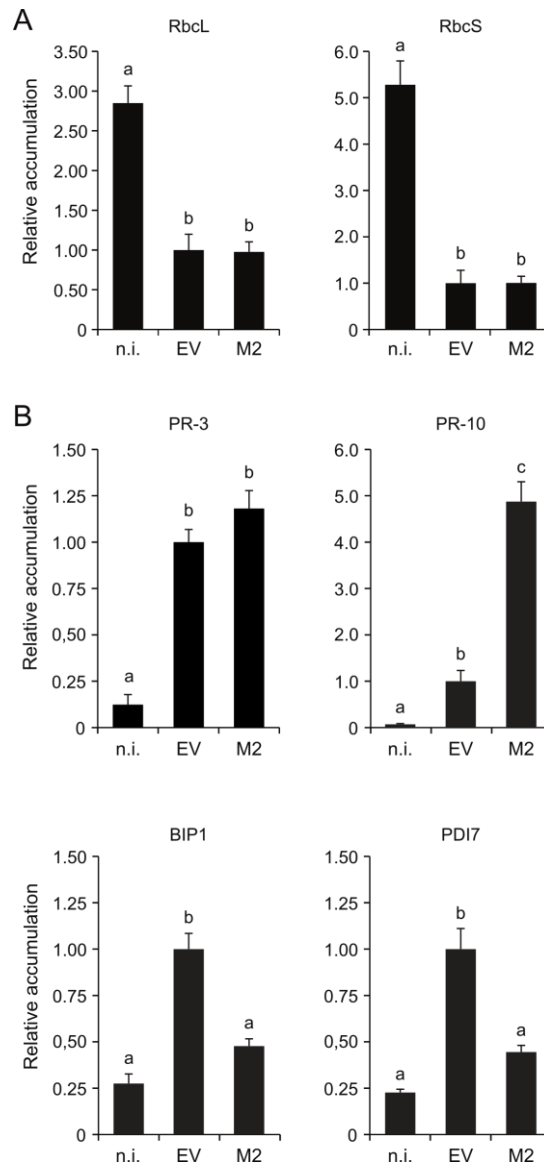
803



804

805 **Figure 6.** Relative abundance of Rubisco subunits and PR proteins in non-infiltrated (n.i.), EV-
806 infiltrated and M2-expressing leaves. (A) Relative abundance of Rubisco large (RbcL) and small
807 (RbcS) subunits. (B) Relative abundance of PR-2 (β -glucanase) and PR-3 (chitinase) isoforms.
808 Data are expressed relative to EV-infiltrated leaves (arbitrary value of 1). Each bar is the mean of
809 three biological (plant) replicate values \pm SE. Bars with the same letter are not significantly different
810 (post-ANOVA LSD; $P=0.05$).

811

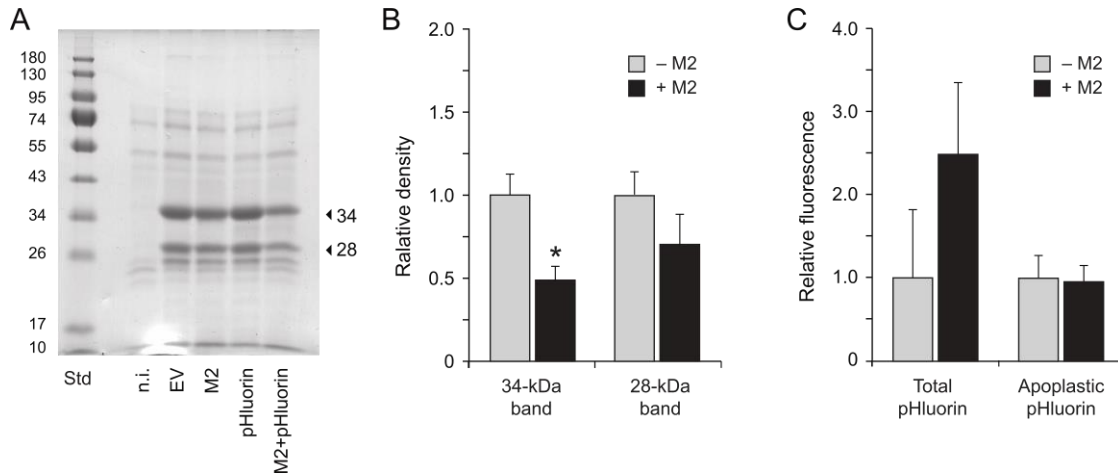


812

813 **Figure 7.** RT-qPCR analysis of Rubisco and defense-related protein transcripts in RNA extracts
814 of non-infiltrated (n.i.), EV-infiltrated and M2-expressing leaves. (A) Relative abundance of
815 transcripts for the large (RbcL) and small (RbcS) subunits of Rubisco. (B) Relative abundance of
816 transcripts for PR-3 protein endochitinase A (UniProt Accession P08252), PR-10 protein (UniProt
817 Accession A0A068JKR2), ER chaperone-associated protein BIP1 and protein disulfide isomerase
818 PDI7. Data are expressed relative to EV-infiltrated leaves (arbitrary value of 1.0). Each bar is the
819 mean of four biological (plant) replicate values \pm SE. Bars with the same letter are not significantly
820 different (post-ANOVA LSD; $P=0.05$). Details on DNA primers for the qPCR amplifications are
821 provided in **Supplemental Table S9**.

Philippe V. Jutras et al.

822



823

824 **Figure 8.** Protein secretion in the apoplast of non-infiltrated (n.i.), EV-infiltrated and M2 vector-
825 infiltrated leaves expressing or not reporter protein pHluorin. (A) Apoplastic protein profiles
826 following 12% w/v SDS-PAGE and Coomassie blue staining. Arrows point to the 28- and 34-kDa
827 PR protein isoforms immunodetected above with anti-PR-2 and anti-PR-3 antibodies (**Fig. 6B**).
828 Numbers on the left refer to commercial molecular weight standards (Std). (B) Abundance of the
829 28-kDa and 34-kDa PR proteins in apoplast protein preparations of agroinfiltrated leaves
830 expressing (+M2) or not (-M2) the M2 channel. Abundance values were inferred from the volumic
831 densities of Coomassie blue-stained 28-kDa and 34-kDa bands following SDS-PAGE (see panel
832 A). Data are expressed relative to mean density values in apoplast extracts of '-M2' (EV, pHluorin)
833 infiltrated leaves. (C) Fluorescence emission at 520 nm in whole cell (Total) and apoplast protein
834 extracts of agroinfiltrated leaves expressing pHluorin alone (-M2) or along with M2 (+M2). Data
835 are expressed relative to fluorescence emitted in leaf extracts expressing pHluorin alone (-M2).
836 Each bar is the mean of three biological (plant) replicates \pm SE.